Electronic Supplementary Material (ESI) for Materials Advances.

Supporting Information

Mixed dimensionality of 2D/3D heterojunction for improving charge transport and long-term stability in high-efficiency 1.63-eV bandgap perovskite solar cells

*Jinkun Jiang[a], Congcong Tian[a], Zhiang Zhang[a], Xiao (Xiao) Liu[a], Xin Wang[a], Yiting Zheng[a], Zhanfei Zhang[a], Luyao Wang[a], Xueyun Wu[a], Jianghu Liang[a], Chun-Chao Chen[a]**

[a]School of Materials Science and Engineering, Shanghai Jiao Tong University, Shanghai, 200240, P. R. China

*Corresponding author: c3chen@sjtu.edu.cn

Experimental section

Materials. Lead iodide (PbI_2), lead bromide ($PbBr_2$), methylammonium bromide (MABr), lithium bis (trifluoromethylsulphonyl) imide (Li-TFSI), and 2,2′,7,7′-tetrakis-(N,N-di-p-methoxyphenylamine)-9,9′-spirobifluorene (Spiro-OMeTAD) were purchased from Xi'an Polymer Light Technology. Cesium iodide (CsI), rubidium iodide (RbI), N,N-dimethylformamide (DMF), chlorobenzene (CB), and 4-tert-butylpyridine (4-tBP) were purchased from Sigma-Aldrich. R-α-methylbenzylamine, R-α-methyl-4-fluorobenzylammonium hydrochloride (R-α-FMBACl), and dimethyl sulfoxide (DMSO) were purchased from Meryer. Acetonitrile was purchased from Aladdin. Formamidinium iodide (FAI) was purchased from Greatcell. R-α-methyl-4-chlorobenzylammonium hydrochloride (R-α-ClMBACl) was purchased from Leyan. R-α-methyl-4-bromobenzylammonium hydrochloride (R-α-BrMBACl) was purchased from Macklin. Isopropanol (IPA) was purchased from J&K Scientific. Hydrochloric acid (HCl) and ether were purchased from Sinopharm Chemical Reagent. Ethanol was purchased from Energy Chemical. [6,6]-phenyl-C61-butyric acid methyl ester (PCBM) was purchased from Liaoning Tech. Tin oxide colloid precursor (SnO_2) was purchased from Alfa Aesar. All above materials were used without further purification.

Synthesis of R-α-MBACl. R-α-MBACl was synthesized by reacting R-α-methylbenzylamine and HCl (molar ratio 1:1) in ethanol at 0 °C for 4 h with stirring. The precipitates were recovered by evaporating the solution at 50 °C for 1 h. The product was dissolved in ethanol, recrystallized from diethyl ether, and finally dried at 60 °C in a vacuum oven for 24 h.

Device fabrication. FTO glass was cleaned through sonication in IPA, detergent, deionized water, acetone, and IPA, respectively. Before use, the FTO substrates were dried with air gas and treated by UV-ozone for 15 min. SnO_2 thin film was prepared by spin-coating colloidal solution on the FTO substrates at 3000 rpm in ambient air, then annealed on a hot plate at 150 ℃. Perovskite precursor solution $Rb_{0.05}Cs_{0.05}(FAPbI_3)_{0.87}(MAPbBr_3)_{0.13}$ (1.3 M) was spin-coated on the SnO_2 substrates at 5000 rpm for 35 s. CB was dropped on the spinning substrates during the last 5 s. Subsequently, the films were annealed at 100 °C to form perovskites. The solution of different organic ligands (R-α-MBA, R-α-FMBA, R-α-ClMBA, R-α-BrMBA) at 4 mg/mL in IPA was spin-coating onto the perovskite films, and then annealed on a hot plate at 100 ℃ for 10 min. Spiro-OMeTAD solution containing 72.3 mg Spiro-OMeTAD, 17.5 μL Li-TFSI solution (520 mg Li-TFSI in acetonitrile), and 30 μL 4-tBP in 1mL CB was spin-coated on the perovskite films. Finally, 100 nm of Ag electrode was deposited on the film through thermal evaporation under vacuum of 1×10^{-5} Pa. The accurate active cell area was 0.09959 cm^2 defined a non-reflective mask for the efficiency measurement.

Characterization. X-ray diffraction (XRD) patterns were conducted employing a D8 ADVANCE Da Vinci diffractometer and Cu-Kα radiation with the scanning rate of 10°/min. The top-view and cross-sectional morphologies were characterized by a JSM-

7800F scanning electron microscopy (SEM). Roughness of the films was acquired via a FastScan Bio Atomic Force Microscope (AFM). Steady-state photoluminescence (PL) and time-resolved photoluminescence (TRPL) spectra were performed with a FLS1000 PL spectrometer with an excitation at 450 nm. Transient absorption (TA) was conducted on a Ultrafast Systems LLC Helios pump-probe system combined with an amplified femtosecond laser system. Ultraviolet-visible (UV-vis) absorption spectra were acquired by a EV300 UV-vis spectrophotometer. X-ray photoelectron spectroscopy (XPS) and ultroviolet photoelectron spectroscopy (UPS) were obtained on a AXIS UltraDLD spectrometer. Current density-voltage (*J-V*) curves of the PSCs were measured using a Keithley 2400 source meter under 1 sun illumination at 100 mW cm^{-2} (AM 1.5G) using an Abet Technologies Sun 2000 solar simulator. The light intensity was calibrated using a standard silicon reference cell. Both of the reverse (1.2 V to -0.1 V) and forward (-0.1 V to 1.2 V) scans were measure using a scan rate of 0.02 V s^{-1}. Current density-time (J_{SC}-t), power conversion efficiency-time (PCE-t), space charge-limited current (SCLC), and dark *J-V* curves were measured on the Keithley 2400 source meter. External Quantum Efficiency (EQE) spectra were recorded via a Qtest Hifinity 5 EQE measurement system. Electrochemical Impedance Spectroscopy (EIS) and Mott-Schottky (M-S) curves were performed using a CorrTest CS350M electrochemical workstation. Water contact angle was obtained by a DSA100 instrument.

Computational details. First-principles calculations based on the density functional theory were implemented in the Vienna ab initio simulation package.[1, 2] Perdew-Burke-Ernzerh (PBE) functional within the generalized gradient approximation (GGA) was select as the exchange-correlation function.[3] The valence-core interactions were described via the projector-augmented-wave (PAW) pseudopotentials.[4] A plane-wave cut-off energy of 500 eV was used. The energy and force convergence criteria were set to 10^{-5} eV and 0.02 eV $Å^{-1}$, respectively. The formation energy of n = 1 2D perovskites was calculated as the following fomula: $E_{formation}(2D) = E_{DFT}(2D) - 2E_{DFT}(XMBA) - E_{DFT}(PbI_2)$. Iodide migration activation energy was modeled for $MAPbI_3$, $MBAPbI_3$ and $BrMBAPbI_3$ in which the MA cation was replaced by a MBA/BrMBA cation in a single cell for the latter two cases. The parameters of the perovskite surface model were 6Å×6 Å×14 Å. The thickness of the vacuum layer is 10 Å. The *k*-points grid sampling size was set as 2 × 2 × 1 in the Brillouin Zone. V_I vacancy was initially set corresponding to the defect in the initial and final structure respectively. After the initial and final structures were optimized, a linear interpolation consisting of ten grid points between them were employed to define the migration process. The energy profiles were examined using climbing-nudged elastic band (Cl-NEB) and constrained energy minimization methods.

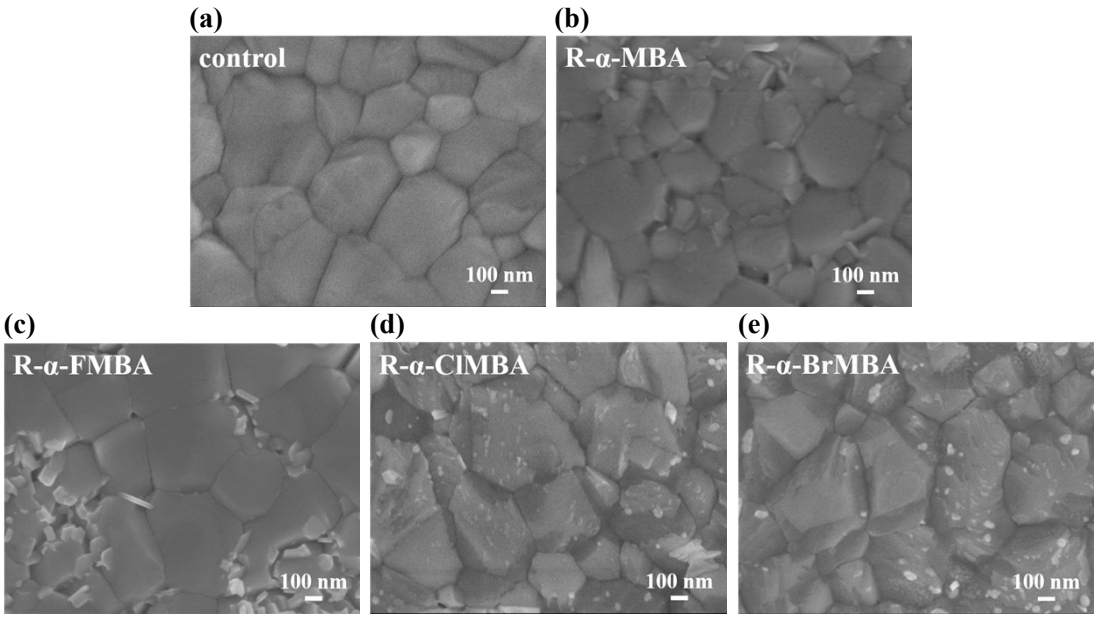

Figure S1. SEM images of surface morphology for perovskite films modified with different ligands (a) control, (b) R-α-MBA, (c) R-α-FMBA, (d) R-α-ClMBA and (e) R-α-BrMBA.

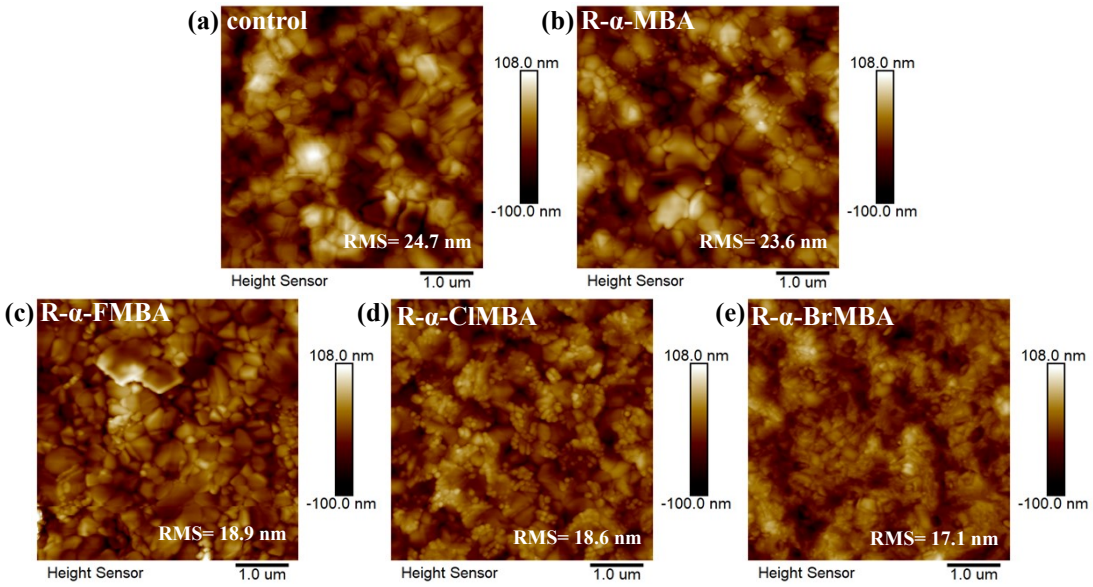

Figure S2. AFM images of perovskite films modified with different ligands (a) control, (b) R-α-MBA, (c) R-α-FMBA, (d) R-α-ClMBA and (e) R-α-BrMBA.

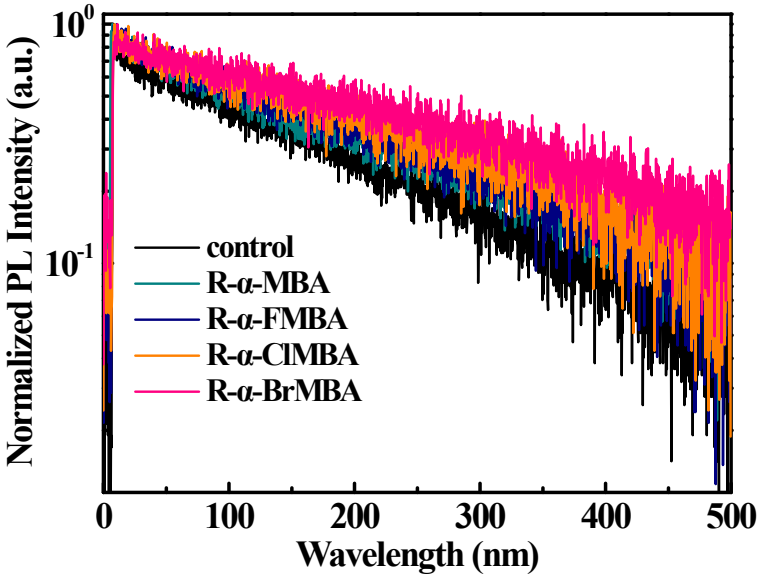

Figure S3. TRPL spectra of perovskite films modified with different organic ligands.

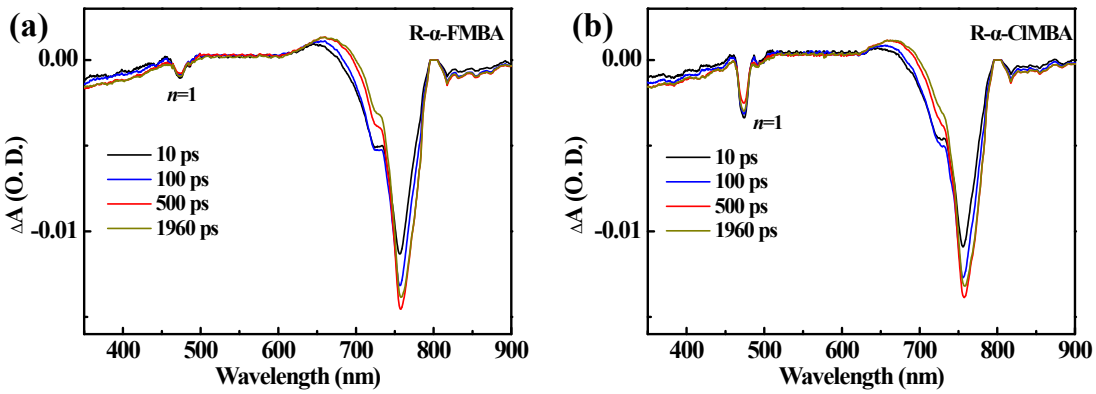

Figure S4. TA spectra for the (a) R-α-FMBA- and (b) R-α-ClMBA-modified perovskite films.

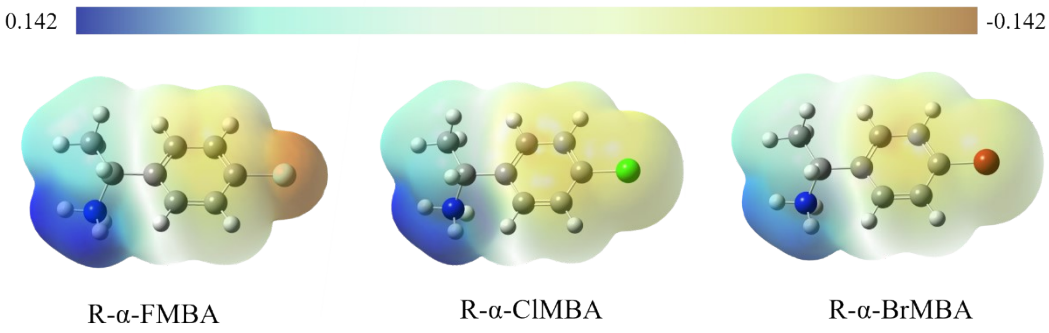

Figure S5. Electrostatic surface potential maps of the halogen-substituted aromatic ligands.

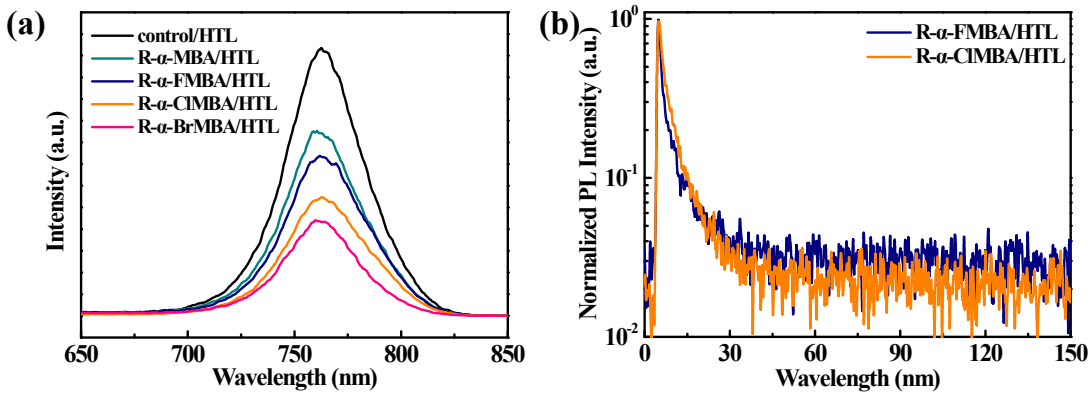

Figure S6. (a) Steady-state PL spectra of perovskite/HTL films with and without modification. (b) TRPL spectra of perovskite/HTL films modified with R-α-FMBA and R-α-BrMBA.

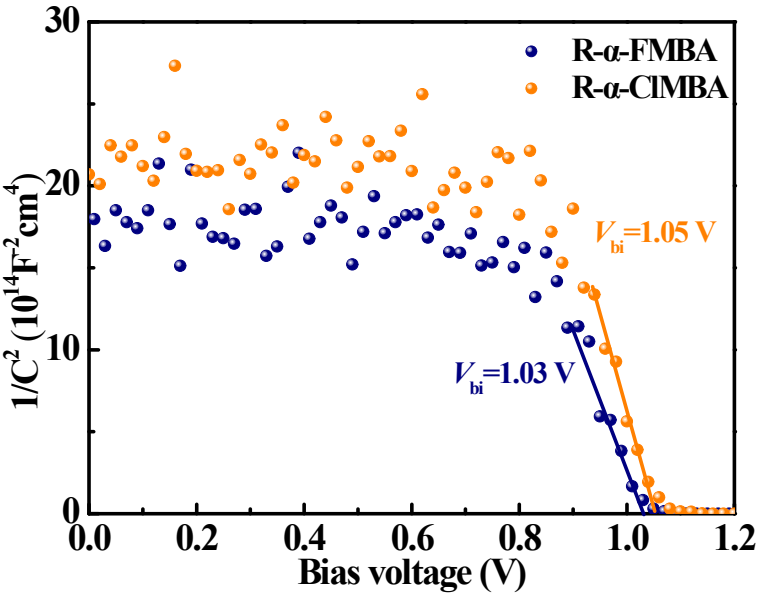

Figure S7. Mott-Schottky curves for different perovskite devices.

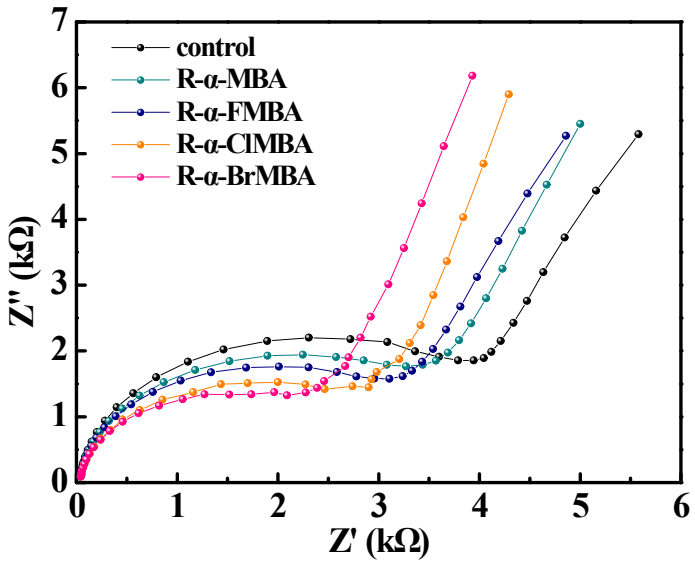

Figure S8. Nyquist plots of different perovskite devices.

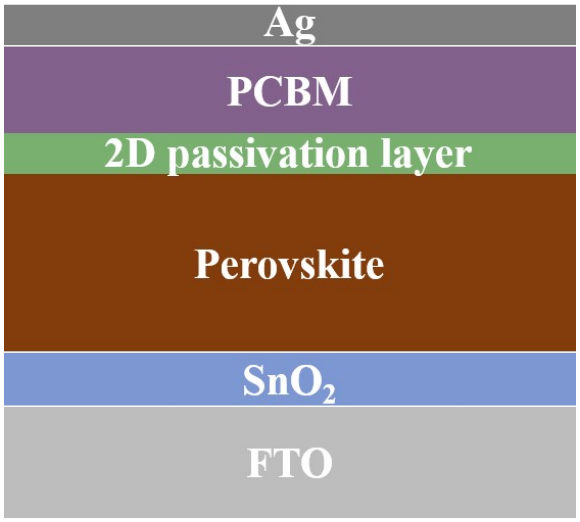

Figure S9. Schematic diagram of electron-only device.

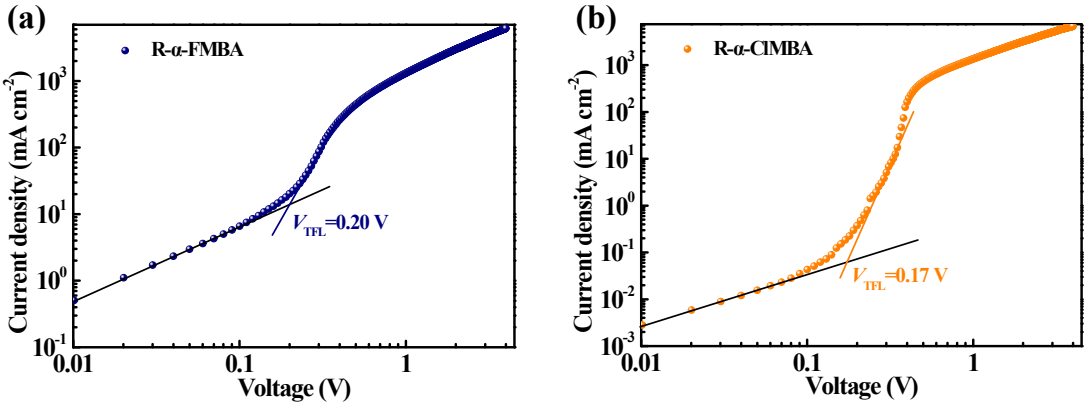

Figure S10. SCLC curves for different perovskite devices.

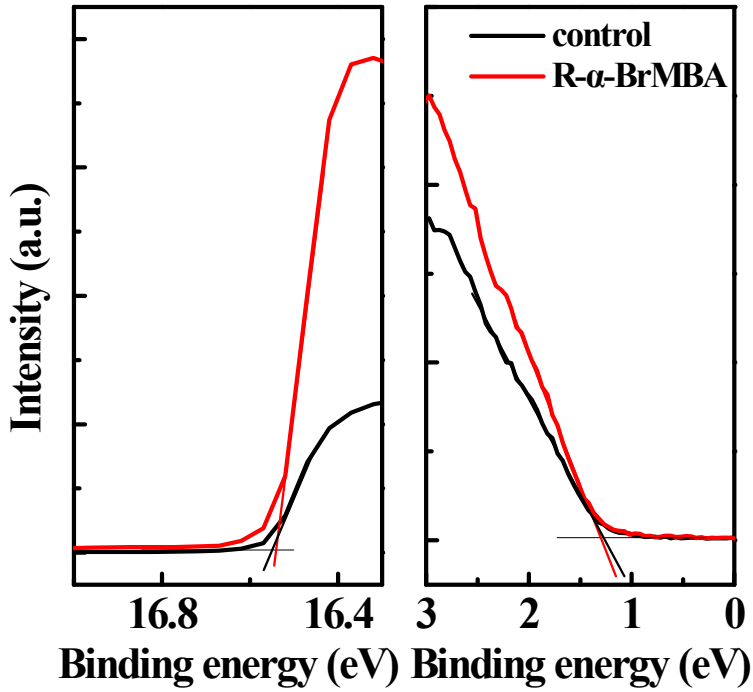

Figure S11. UPS spectra of secondary electron cutoff and valence band of the 3D and Br-2D/3D films.

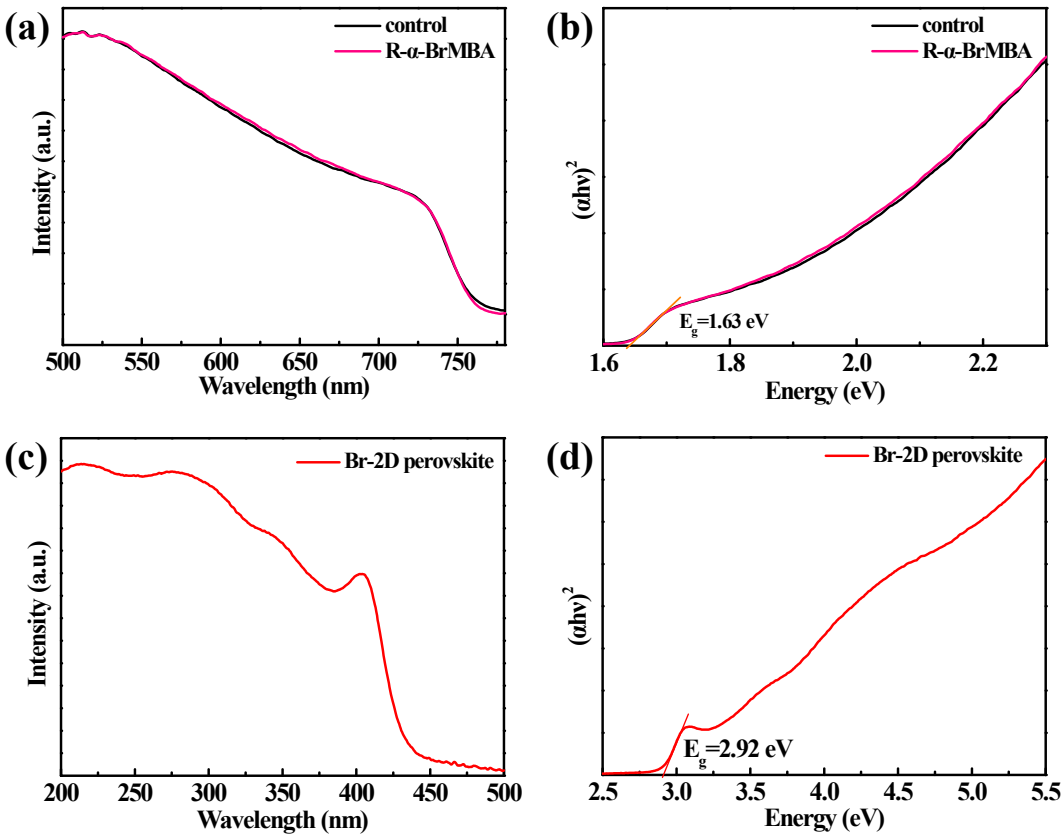

Figure S12. UV-vis spectra of (a) perovskite films with and without R-α-BrMBA modification and (c) Br-2D perovskite film. Tauc plots of the (b) 3D and Br-2D/3D films and (d) Br-2D perovskite film.

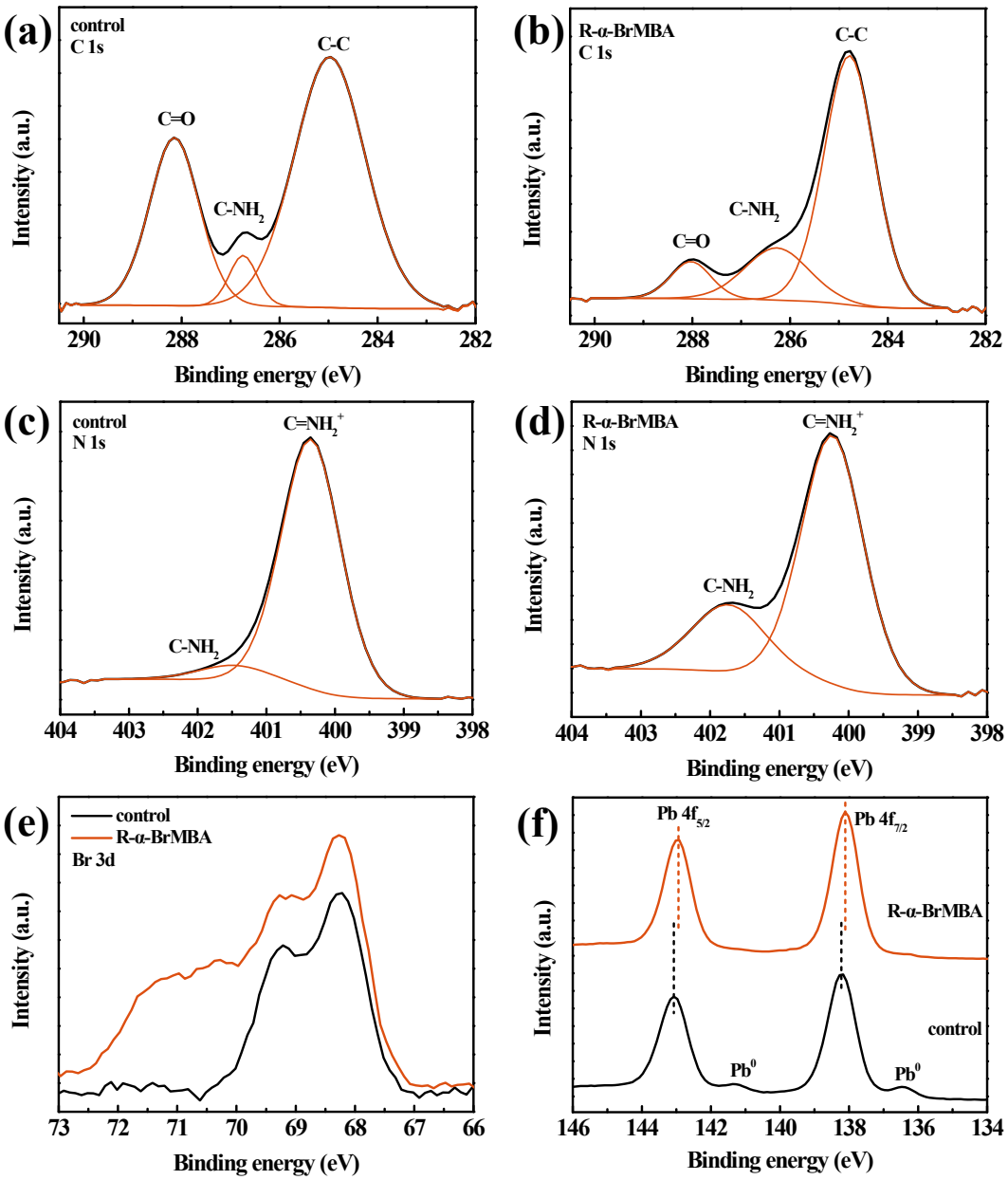

Figure S13. XPS spectra of (a) C 1s for 3D perovskite film, (b) C 1s for Br-2D/3D perovskite film, (c) N 1s for 3D perovskite film, (d) N 1s of Br-2D/3D perovskite film, (f) Br 3d for 3D and Br-2D/3D perovskite films, and (f) Pb 4f for 3D and Br-2D/3D perovskite films.

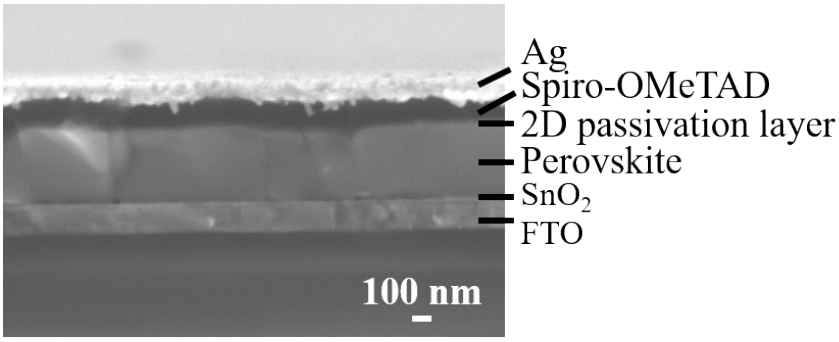

Figure S14. Cross-sectional SEM image of device.

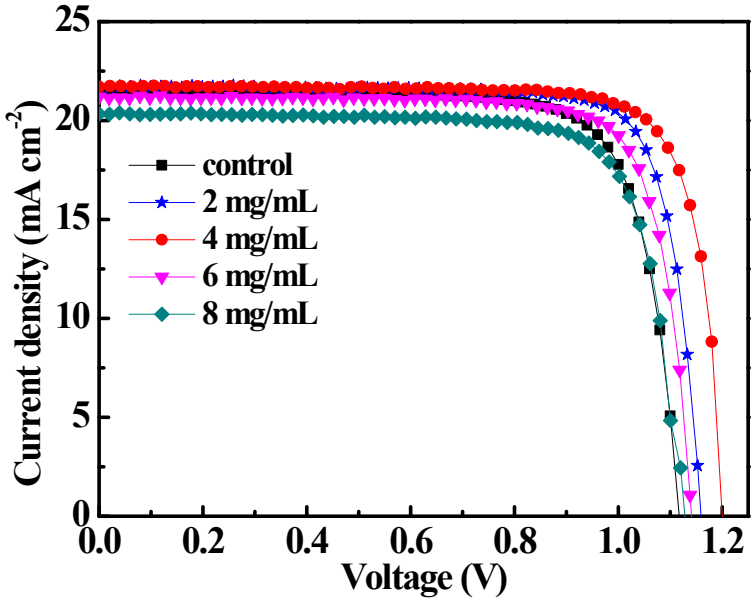

Figure S15. *J-V* curves of PSCs modified with different concentration of R-α-BrMBA.

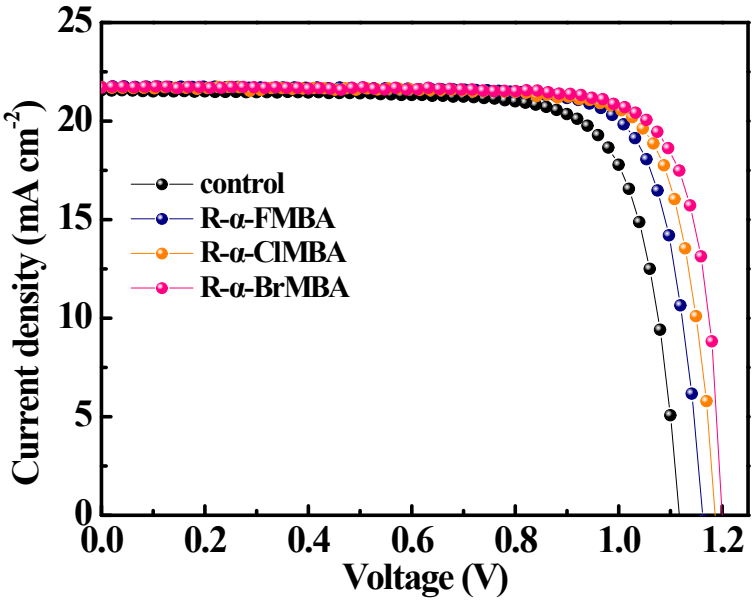

Figure S16. *J-V* curves of PSCs modified with different halogen-substituted ligands.

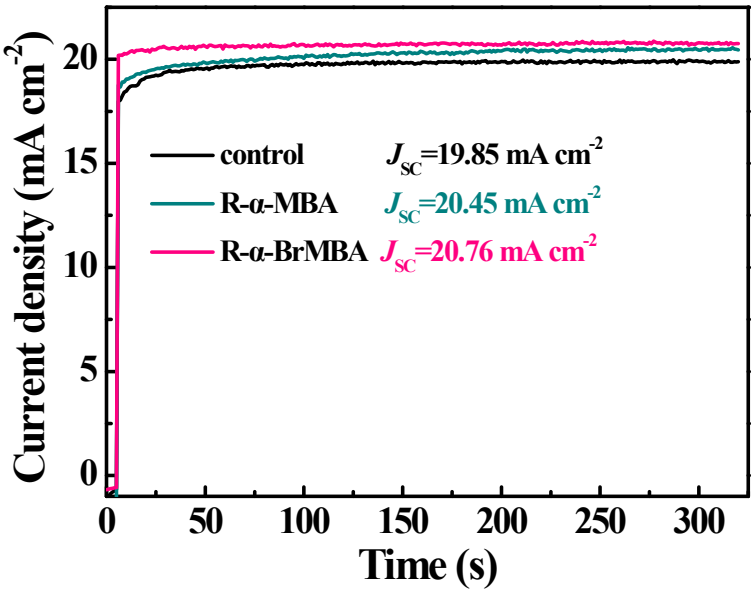

Figure S17. Steady-state current density of perovskite devices with different modification.

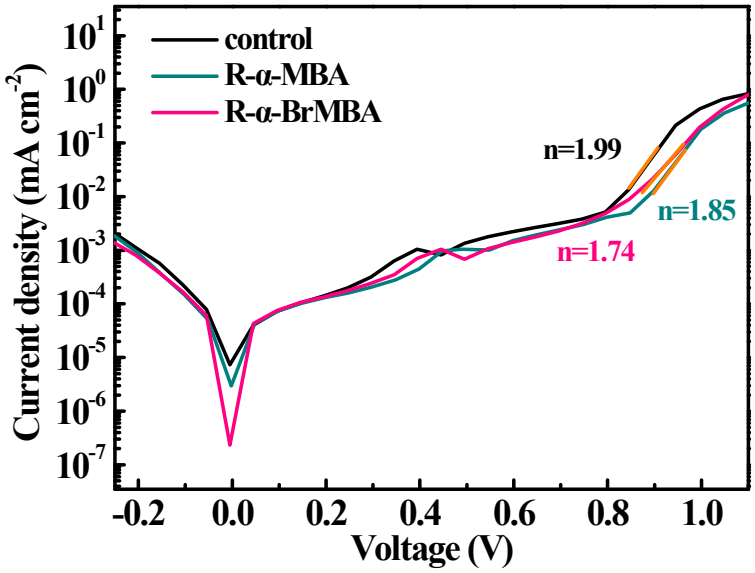

Figure S18. Dark J-V curves of different PSCs.

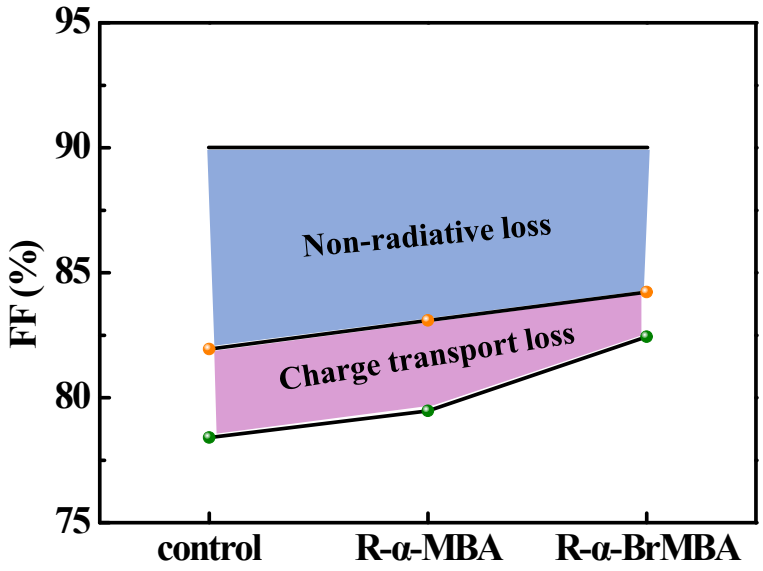

Figure S19. The device FF loss consists of non-radiative loss (blue region) and charge transport loss (purple region), the green and the orange circles represent the measured FF and the calculated FF maximum without charge transport loss, respectively.

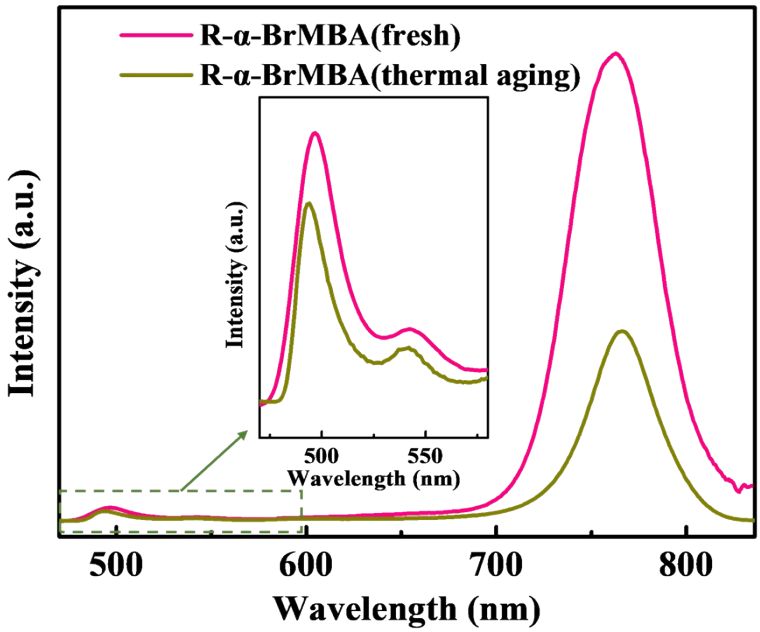

Figure S20. PL spectra of fresh and thermal aged (annealed at 60 ℃ for 8 days) perovskite films modified with R-α-BrMBA.

Table S1. TRPL decay curves fitted results of perovskite films modified with different organic ligands

Samples	τ_1 (ns)	τ_2 (ns)	A_1 (%)	A_2 (%)	τ_{avg} (ns)
Control	9.54	221.96	0.63	99.37	221.90
R-α-MBA	41.83	307.10	4.56	95.44	305.38
R-α-FMBA	31.14	315.48	1.58	98.42	315.03
R-α-ClMBA	43.90	470.72	0.78	99.22	470.41
R-α-BrMBA	17.13	541.36	0.19	99.81	541.33

Table S2. TRPL decay curves fitted results of perovskite/Spiro-OMeTAD films modified with different ligands

Samples	τ_1 (ns)	τ_2 (ns)	A_1 (%)	A_2 (%)	τ_{avg} (ns)
Control	3.13	13.38	35.38	64.62	12.72
R-α-MBA	1.35	9.55	33.37	66.63	9.02
R-α-FMBA	0.84	7.35	30.09	69.91	7.04
R-α-ClMBA	1.6	7.06	32.00	68.00	6.53
R-α-BrMBA	0.7	5.78	16.72	83.28	5.65

Table S3. Values of R_{ct} and R_{rec} calculated from the EIS plots

Samples	R_{ct} (kΩ)	R_{rec} (kΩ)
Control	4.66	31.7
R-α-MBA	4.06	59.36
R-α-FMBA	4.00	98.50
R-α-ClMBA	3.64	251.16
R-α-BrMBA	3.22	299.10

Table S4. The charge mobility (μ) and trap density (N_t) of different devices calculated from SCLC curves

Samples	V_{TFL} (V)	N_t (× 10^{15} cm^{-3})	μ (× 10^{-2} $cm^2V^{-1}s^{-1}$)
Control	0.28	9.08	1.38
R-α-MBA	0.22	7.13	1.62
R-α-FMBA	0.20	6.16	1.79
R-α-ClMBA	0.17	4.86	1.85
R-α-BrMBA	0.14	4.22	1.97

Table S5. Photovoltaic parameters for PSCs modified with different concentration of R-α-BrMBA

Samples	V_{OC} (V)	J_{SC} (mA cm^{-2})	FF (%)	PCE (%)
Control	1.12	21.60	78.41	18.97
2 mg/mL	1.16	21.74	81.27	20.49
4 mg/mL	1.20	21.71	82.44	21.48
6 mg/mL	1.14	21.25	79.96	19.37
8 mg/mL	1.12	20.39	77.92	17.79

Table S6. Photovoltaic parameters for PSCs modified with different halogen-substituted ligands

Samples	V_{OC} (V)	J_{SC} (mA cm^{-2})	FF (%)	PCE (%)
Control	1.12	21.60	78.41	18.97
R-α-FMBA	1.16	21.67	80.82	20.32
R-α-ClMBA	1.18	21.69	81.54	20.87
R-α-BrMBA	1.20	21.71	82.44	21.48

Table S7. Reported Performance of the quadruple-cation (RbCsFAMA) PSCs

Year	PCE(%)	V_{OC}(V)	FF(%)	Passivation Method	Stability (% of PCE after # of hours at %RH/℃)	Ref
2016	21.60	1.18	81.00	None	95% /500h/85°C/Nitrogen glovebox	Ref.[5]
2017	21.10	1.16	78.00	None	None	Ref.[6]
2018	20.86	1.21	76.10	Interfacial engineering	None	Ref.[7]
2019	20.92	1.12	79.00	Additive engineeing	95%/96h/40±5%RH/ unencapsulated	Ref.[8]
2020	20.92	1.14	79.82	Interfacial engineering	83%/480h/30%RH unencapsulated	Ref.[9]
2021	17.71	1.19	80.30	Interfacial engineering	90%/500h/30±5%RH unencapsulated	Ref.[10]
2021	20.35	1.13	81.53	two-step sequential deposition	86%/672h/20%RH/25℃ unencapsulated	Ref.[11]
2021	21.54	1.24	77.65	Interfacial engineering	100%/45days/30%RH/ unencapsulated	Ref.[12]
2021	21.56	1.21	80.11	Interfacial engineering	70%/720h/30±5%RH/ unencapsulated	Ref.[13]
2022	21.48	1.20	82.44	Interfacial engineering	90%/1000h/35±5%RH/ unencapsulated 87%/216h/60℃/ unencapsulated	This work

References

1. G. Kresse, *Phys. Rev. B*, 1996, **54**, 11169.
2. G. Kresse and J. Furthmiiller, *Comput. Mater. Sci.*, 1996, **6**, 15-50.
3. J. P. Perdew, K. Burke and M. Ernzerhof, *Phys. Rev. Lett.*, 1996, **77**, 3865.
4. P. E. Blochl, *Phys. Rev. B* 1994, **50**, 17953-17979.
5. M. Saliba, T. Matsui, K. Domanski, J.-Y. Seo, A. Ummadisingu, S. M. Zakeeruddin, J.-P. Correa-Baena, W. R. Tress, A. Abate, A. Hagfeldt and M. Grätzel, *Science*, 2016, **354**, 206-209.
6. P. Yadav, M. I. Dar, N. Arora, E. A. Alharbi, F. Giordano, S. M. Zakeeruddin and M. Gratzel, *Adv. Mater.*, 2017, **29**, 1701077.
7. J. Peng, J. I. Khan, W. Liu, E. Ugur, T. Duong, Y. Wu, H. Shen, K. Wang, H. Dang, E. Aydin, X. Yang, Y. Wan, K. J. Weber, K. R. Catchpole, F. Laquai, S. Wolf and T. P. White, *Adv. Energy Mater.*, 2018, **8**, 1801208.

8. J. V. Patil, S. S. Mali and C. K. Hong, *Nanoscale*, 2019, **11**, 21824-21833.
9. X. Liu, Y. Cheng, B. Tang, Z. G. Yu, M. Li, F. Lin, S. Zhang, Y.-W. Zhang, J. Ouyang and H. Gong, *Nano Energy*, 2020, **71**, 104556.
10. K. M. Reza, A. Gurung, B. Bahrami, A. H. Chowdhury, N. Ghimire, R. Pathak, S. I. Rahman, M. A. R. Laskar, K. Chen, R. S. Bobba, B. S. Lamsal, L. K. Biswas, Y. Zhou, B. Logue and Q. Qiao, *Sol. RRL*, 2021, **5**, 2000740.
11. X. Liu, Z. Wu, X. Fu, L. Tang, J. Li, J. Gong and X. Xiao, *Nano Energy*, 2021, **86**, 106114.
12. G. Yang, Z. Ren, K. Liu, M. Qin, W. Deng, H. Zhang, H. Wang, J. Liang, F. Ye, Q. Liang, H. Yin, Y. Chen, Y. Zhuang, S. Li, B. Gao, J. Wang, T. Shi, X. Wang, X. Lu, H. Wu, J. Hou, D. Lei, S. K. So, Y. Yang, G. Fang and G. Li, *Nat. Photonics*, 2021, **15**, 681–689.
13. Z. Zhang, J. Jiang, X. Xiao Liu, X. Wang, L. Wang, Y. Qiu, Z. Zhang, Y. Zheng, X. Wu, J. Liang, C. Tian and C. C. Chen, *Small*, 2022, **18**, e2105184.